Supporting Information

Flexible Zinc-Air Batteries with One-Step Gel Electrolyte Featuring High Performance and Environmental Adaptability

Zisen Ye, [†a] Wenhui Guo, [†a, b] Yang Chen, [a] Mingcheng Yang, [a] Benshang Zhang, [a] Shubo Liu, [a] and Yaxin Guo[a]*

a. Institute of Isotope, Henan Academy of Sciences Co., Ltd, Zhengzhou 450015, Henan, China

b. School of Chemical Engineering Zhengzhou University, Zhengzhou 450015, Henan, China

Experimental section

Materials

Acrylic acid (AA, analytically pure, 99%), potassium hydroxide (KOH, analytically pure, 95%), Quaternized chitosan (QCS, degree of substitution: 90%), sodium chloride (NaCl, analytically pure, 99%), N,N'-methylenebisacrylamide (MBAA, 98%), and potassium persulfate (KPS, 98.5%) were all purchased from Aladdin Reagent Co., Ltd. and used as received without further purification. The air cathodes were purchased from Wenyan Scientific Co., Ltd., composed of a nickel foam substrate loaded with Co_2O_3 as the active material. Zinc foil (thickness: 1 mm) was obtained from Saibao Battery Materials Co., Ltd.

Preparation of QCS-PAA-NaCl

The QCS-PAA-NaCl gel electrolyte was prepared via in-situ polymerization in alkaline media. First, 50 mL of a mixed solution containing 7.5 mol L^{-1} KOH and 0.3 mol L^{-1} zinc acetate was prepared. Subsequently, 6 mL of AA was added dropwise

under continuous stirring to ensure uniform neutralization and dispersion. Afterward, 1.2 g of QCS was introduced into the system and stirred thoroughly until completely dissolved, followed by the addition of 1.0 g of NaCl. The mixture was then stirred for another 2 h to ensure full ionic distribution. After the mixture became homogeneous, MBAA (0.06 g) was first introduced as the cross-linker and stirred for 1 h to ensure complete dissolution. Subsequently, KPS (0.03 g) was added as the initiator, and the precursor was stirred until a uniform solution was obtained. Finally, the solution was poured into a mold and subjected to thermal polymerization at 50 °C in a vacuum oven to form the QCS-PAA-NaCl gel electrolyte.

For comparison, the QCS-PAA gel electrolyte was prepared using the same procedure, except that NaCl was omitted. The PAA gel electrolyte was prepared similarly but without the addition of QCS.

Assembly of Flexible ZABs

The flexible ZABs were assembled in a sandwich-type configuration using the as-prepared gel electrolyte. The QCS-PAA-NaCl gel electrolyte was cut into rectangular strips with dimensions of 3 cm × 1 cm and a controlled thickness of 5 ± 0.2 mm. Zinc foil (anode) and air cathode were trimmed into rectangular strips with dimensions of 4 cm × 1 cm.

During assembly, the zinc anode, gel electrolyte, and air cathode were sequentially stacked to form a planar sandwich structure. Both electrodes were designed to extend slightly beyond the gel electrolyte at opposite ends, serving as electrical connection terminals for external

testing. The assembled cell was fixed using medical-grade breathable adhesive tape, which ensured uniform and intimate contact between the gel electrolyte and both the zinc anode and air cathode while preserving the overall flexibility of the device. The same fixation and wrapping procedure was consistently applied to all samples to maintain comparable interfacial contact conditions across different cells

Water Retention Test

The water retention properties of the gel electrolytes were evaluated at ambient temperature (20°C) and relative humidity of 40-50%. The synthesized gels were cut into rectangular strips with dimensions of 1 cm × 3 cm. The initial weight of each sample was recorded as M, and the remaining mass m_n was measured every hour (n = 1, 2, 3, ...). The water retention ratio W at each time point was calculated according to the following equation:

$$Wn = \frac{m_n}{M}$$

This test was used to assess the ability of the gel electrolyte to retain moisture over time under ambient conditions.

Ionic Conductivity Test

The ionic conductivity of the gel electrolytes was measured using electrochemical impedance spectroscopy (EIS) on a CHI660E electrochemical workstation. The gel sample was sandwiched between two stainless steel electrodes, ensuring good contact. The Nyquist plot was recorded over a frequency range of 1000 Hz to 1 MHz at open-circuit voltage. In the obtained Nyquist plot, the intercept of the

high-frequency arc on the real axis corresponds to the bulk resistance R of the gel. The thickness of the gel is denoted as h, and A represents the contact area between the gel and the electrodes. The ionic conductivity σ was calculated according to the equation:

$$\sigma = \frac{h}{R \times A}$$

This test was performed at room temperature to evaluate the ion transport capability of the gel electrolytes.

Mechanical Properties Test

The tensile, compressive, and shear adhesion properties of the gel electrolytes were measured using a universal testing machine (AGS-X, Shimadzu, Japan). For the tensile test, gel samples were stretched at a rate of 100 mm min^{-1} until failure. The compressive test was performed at a rate of 1 mm min^{-1} using cylindrical or block-shaped gel samples.

For lap-shear adhesion tests, the gel was sandwiched between two identical substrates (zinc foil or air cathode), with a contact area of 1 cm × 3 cm. The specimens were subjected to tensile loading at a rate of 10 mm min^{-1} until detachment. These tests were used to evaluate the interfacial adhesion between the gel electrolyte and the electrode materials.

Structural and Chemical Characterization

The chemical structure of the hydrogels was analyzed using Fourier-transform infrared spectroscopy (FTIR, TENSOR 27, Bruker) in the wavenumber range of 400-4000 cm^{-1}. The crystalline structure of the freeze-dried hydrogels and post-cycling

zinc anodes was characterized by X-ray diffraction (XRD, Ultima IV, Rigaku) with Cu Kα radiation (λ = 1.5406 Å) over a 2θ range from 10° to 90°. The surface morphology of the freeze-dried gels and zinc electrodes after cycling was examined using a field-emission scanning electron microscope (SEM, Thermo Scientific). The elemental composition and surface chemical states of the gel electrolytes were further investigated using X-ray photoelectron spectroscopy (XPS, K-alpha, Thermo Scientific).

Electrochemical Performance Evaluation of Flexible ZABs

Prior to each electrochemical test, the flexible ZABs were placed in the designated environment for at least 30 min to ensure thermal equilibrium. The electrochemical performance, including rate capability, constant-current discharge, charge–discharge cycling stability, electrochemical impedance spectroscopy (EIS), and power density, was evaluated using a NEWARE multi-channel battery testing system and a CHI660E electrochemical workstation.

For comparative evaluation, flexible ZABs based on different gel electrolytes (PAA, QCS-PAA, and QCS-PAA-NaCl) were fabricated and tested as control and experimental groups under identical conditions. Unless otherwise specified, all electrochemical measurements were carried out using at least five parallel samples (n = 5) for each group to ensure data reliability and reproducibility.

Rate capability was evaluated by stepwise galvanostatic discharge at different current densities. Specifically, the batteries were discharged at each current density for a fixed duration of 10 min, with the current density sequentially increased from

low to high values and then decreased back to a lower current density. The discharge voltages recorded at each step were extracted and combined to construct the rate performance profiles, enabling evaluation of voltage response, polarization behavior, and reversibility under varying current densities.

Cycling stability was assessed using a time-controlled galvanostatic charge-discharge protocol at a constant current density of 2 mA cm^{-2}. In this test, each cycle consisted of 10 min of charging followed by 10 min of discharging, without imposing a fixed voltage cutoff. The total cycling duration and voltage evolution were used to evaluate the long-term operational stability of the flexible ZABs under continuous working conditions.

Temperature-dependent electrochemical tests were conducted in temperature-controlled incubators set at -30 °C, 0 °C, 20 °C, and 50 °C to systematically assess the battery performance under wide-temperature conditions.

Theoretical Calculations

All density functional theory (DFT) calculations were performed using the Gaussian 16 software package. Geometry optimizations were carried out at the B3LYP /def2-TZV level of theory, with the inclusion of Grimme's DFT-D3 dispersion correction to adequately account for van der Waals interactions.[1-4] The default convergence criteria were adopted, specifically a maximum force threshold of 0.00045 Hartree/Bohr and a maximum nuclear displacement of 0.0018 Å. To ensure that the optimized structures correspond to true local minima on the potential energy surface, harmonic vibrational frequency analyses were conducted at the same

theoretical level, confirming the absence of imaginary frequencies ($\nu > 0$ cm^{-1}). Electrostatic potential maps and charge density difference analyses were subsequently performed using the Multiwfn program.[5-7]

Quantitative Evaluation of Process Sustainability

To quantitatively assess the sustainability advantages of the proposed one-step QCS-PAA-NaCl gel preparation, a comparative analysis was conducted against the conventional KOH soaking method based on experimentally controllable and practically relevant parameters rather than a full life-cycle assessment.

For both routes, the gel dimensions were fixed at 3 cm × 1 cm × 0.5 cm, consistent with those used in all electrochemical tests. In the conventional process, the soaking volume, soaking duration (12-24 h), and residual alkaline liquor remaining after gel removal were recorded. The collectable supernatant volume and residual KOH concentration were quantified by direct volume measurement and acid-base titration, respectively. In contrast, for the one-step method, the presence of free alkaline liquid after polymerization was evaluated by visual inspection and centrifugation, with the detection limit defined by the minimum measurable supernatant volume.

Energy consumption during gel preparation was estimated from the heating, polymerization, and drying steps involved in each process, using the rated power and operating time of the corresponding equipment. The total energy input was further normalized by the mass of each gel piece and by the practical discharge energy output (Wh) of the assembled flexible ZABs, enabling a fair comparison of energy efficiency

and waste generation per functional output.

These quantified indicators—including residual alkaline waste, energy consumption per gel and per gram, and waste-liquid generation normalized to battery output—were used as sustainability-related metrics aligned with green chemistry principles of waste minimization and material efficiency. The comparative results are summarized in Table S1.

Figures and captions

Table S1.

Category	Conventional KOH-Soaking Gel (Control)	One-Step QCS-PAA-NaCl Gel (This Work)	Indicator Meaning
Preparation Process	Gel synthesis → soaking in KOH solution for 12-24 h	One-step in-situ polymerization → no post-soaking	Process complexity, energy requirement
Generation of Collectable Waste Solution	Yes (residual KOH solution remaining after soaking)	No measurable liquid phase; supernatant volume < X mL (detection limit)	Waste reduction & environmental friendliness
Gel Size per Piece	3 × 1 × 0.5 cm（after swelling）	3 × 1 × 0.5 cm	Ensures consistent comparison
Mass of Each Gel Piece (g)	1.2 ± 0.15	1.5 ± 0.15	Used for energy normalization
Collectable Supernatant Volume per Piece (mL)	1.20 ± 0.15 (n = 3)	< X (detection limit)	Waste liquid volume
KOH-Equivalent Residual (g/piece)	0.034 ± 0.006 (by titration)	< 0.002 (detection limit)	Chemical hazard, disposal cost
Energy Consumption for Preparation (Wh/piece)	0.82 ± 0.05 (n = 3)	0.47 ± 0.03 (n = 3)	Energy comparison between methods
Energy Consumption per Gram (Wh·g^{-1})	0.164	0.094	Energy efficiency
Waste Liquid per Energy Output (mL·Wh^{-1})	1.20/0.38=3.16	< 0.05/0.41<0.12	LCA-relevant sustainability indicator
Need for Additional	Required (due to non-	Not required (KOH	Not required (KOH

KOH Replenishment During Use	uniform electrolyte uptake)	uniformly integrated in solid matrix)	uniformly integrated in solid matrix)
Potential Environmental Risks	KOH evaporation, strong alkalinity, corrosive handling, waste solution treatment	No external free KOH; stable solid-state environment	Safety & green chemistry compliance

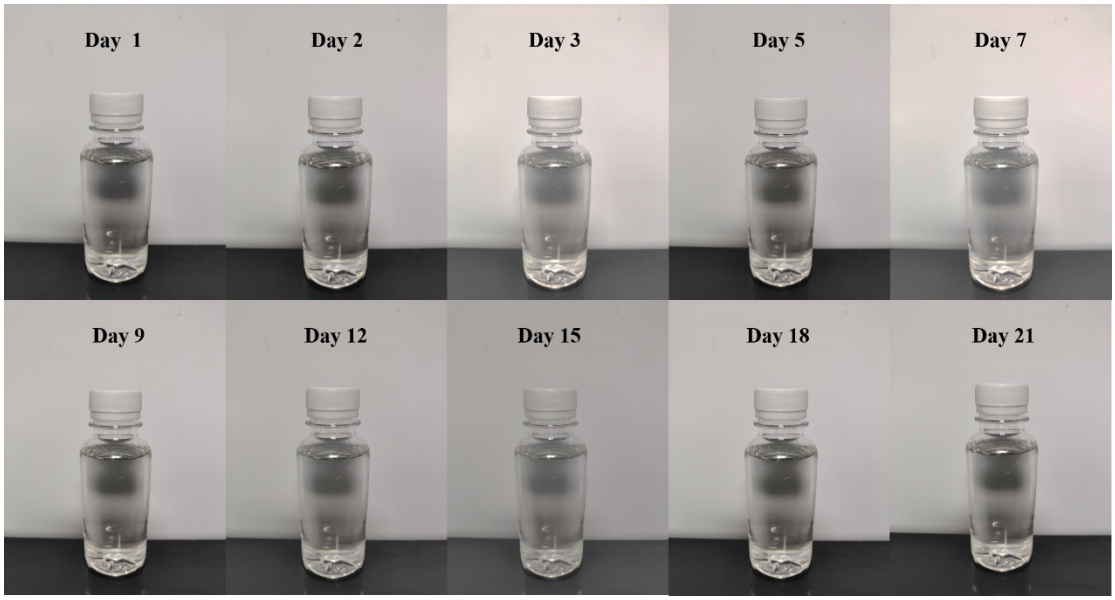

Figure S1. Static states of the mixed solution containing 7.5 mol·L^{-1} KOH and 0.3 mol·L^{-1} zinc acetate after standing for 1-21 days at room temperature (20 °C)

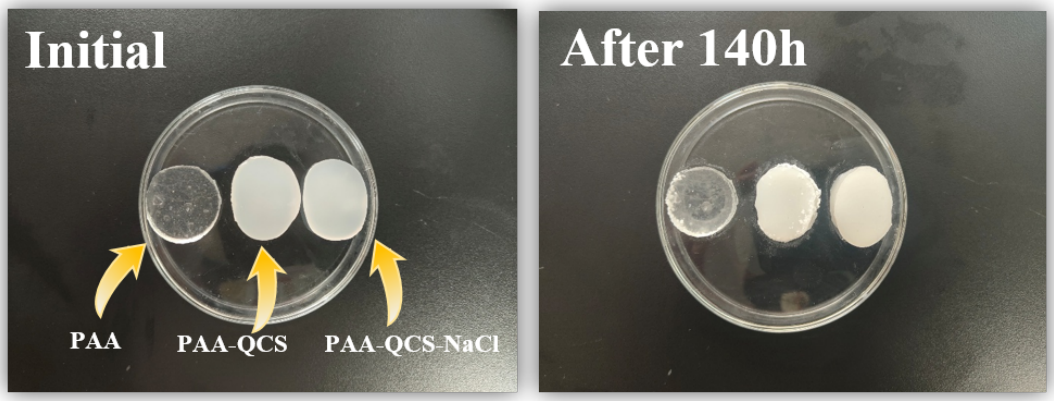

Figure. S2. Time-dependent morphological evolution of the three gel electrolytes, shown by photographs taken at the initial state and after 140 hours of storage under ambient conditions.

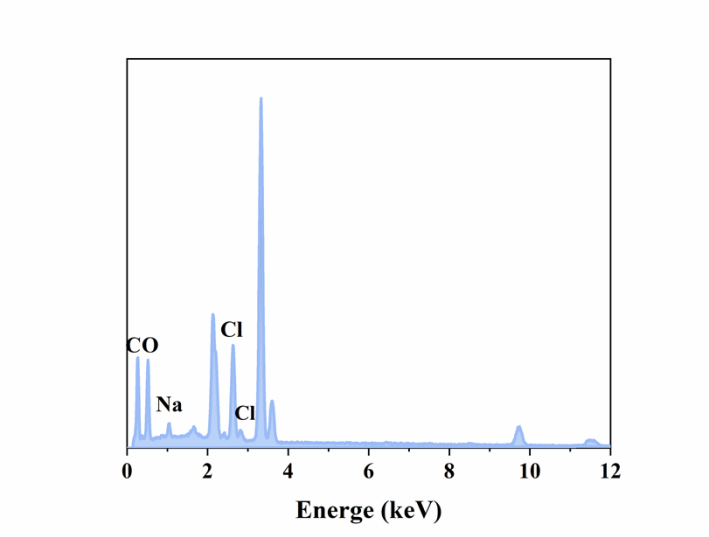

Figure S3. EDS spectrum of PAA-QCS-NaCl hydrogel.

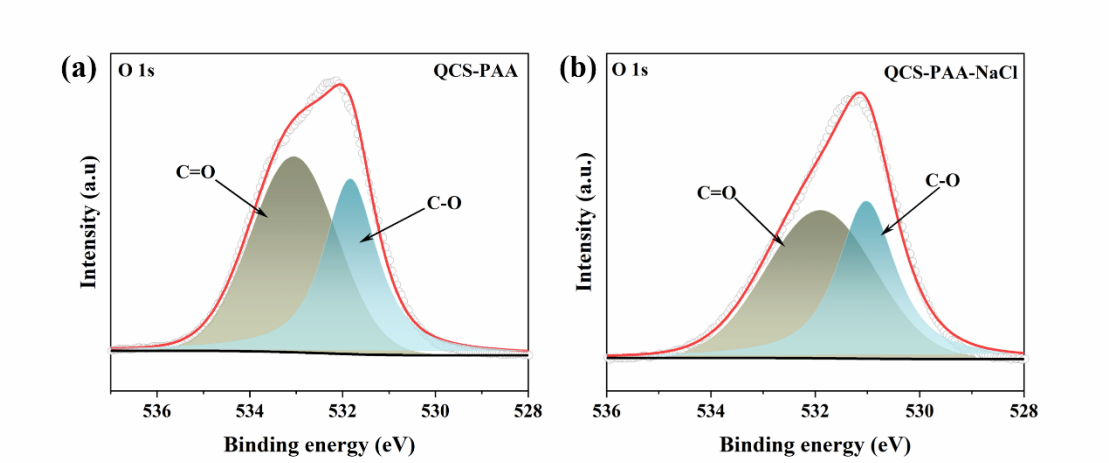

Figure S4. (a) High-resolution O 1s XPS spectrum of the PAA-QCS gel. (b) High resolution O 1s XPS spectrum of the PAA-QCS-NaCl gel.

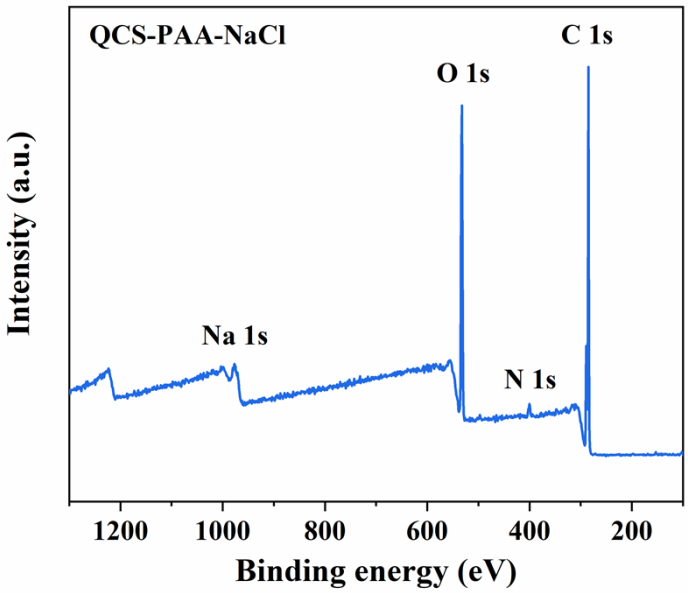

Figure S5. Full XPS spectrum of QCS-PAA-NaCl

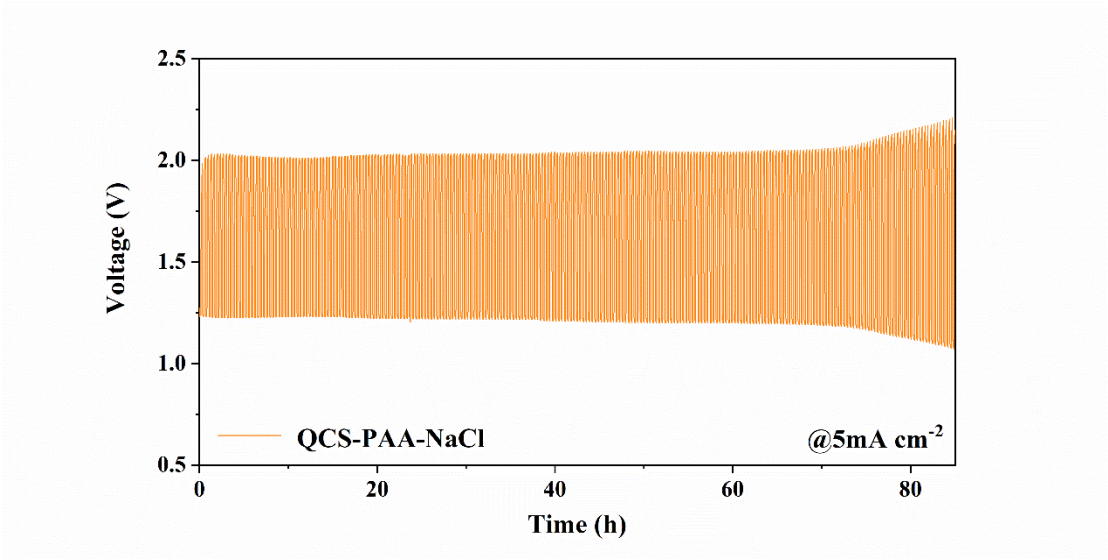

Figure S6. Cycling performance of QCS-PAA-NaCl based flexible ZABs at 5 mA cm^{-2}.

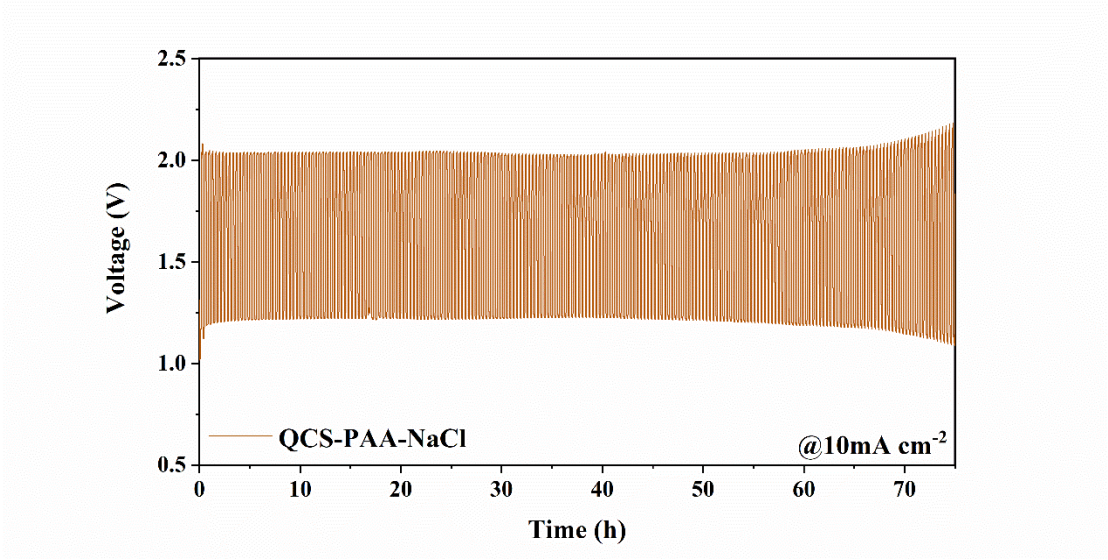

Figure S7. cling performance of QCS-PAA-NaCl based flexible ZABs at 10 mA cm^{-2}.

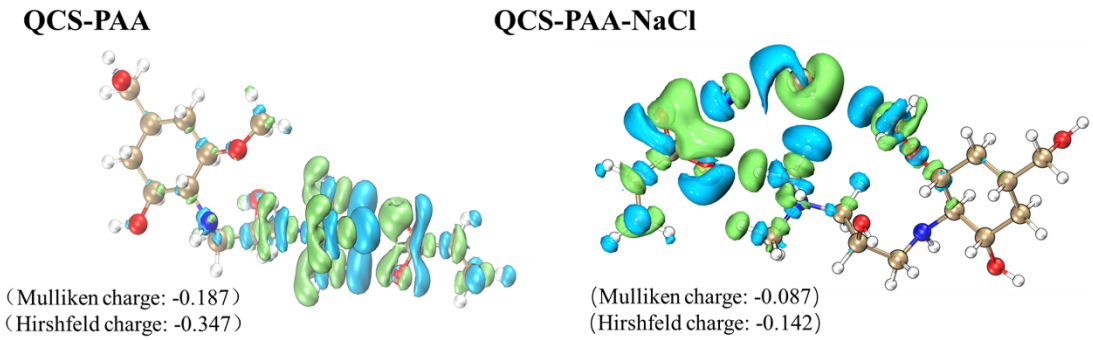

Figure S8. Differential charge density distributions of QCS-PAA and QCS-PAA-NaCl systems.

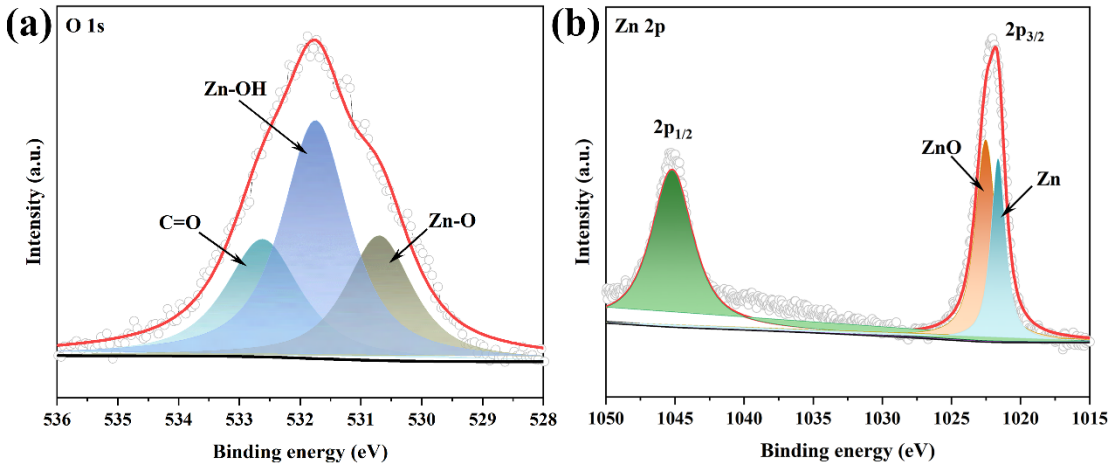

Figure S9. High-resolution XPS spectra of the cycled Zn electrode: (a) O 1s spectrum and (b) Zn 2p spectrum.

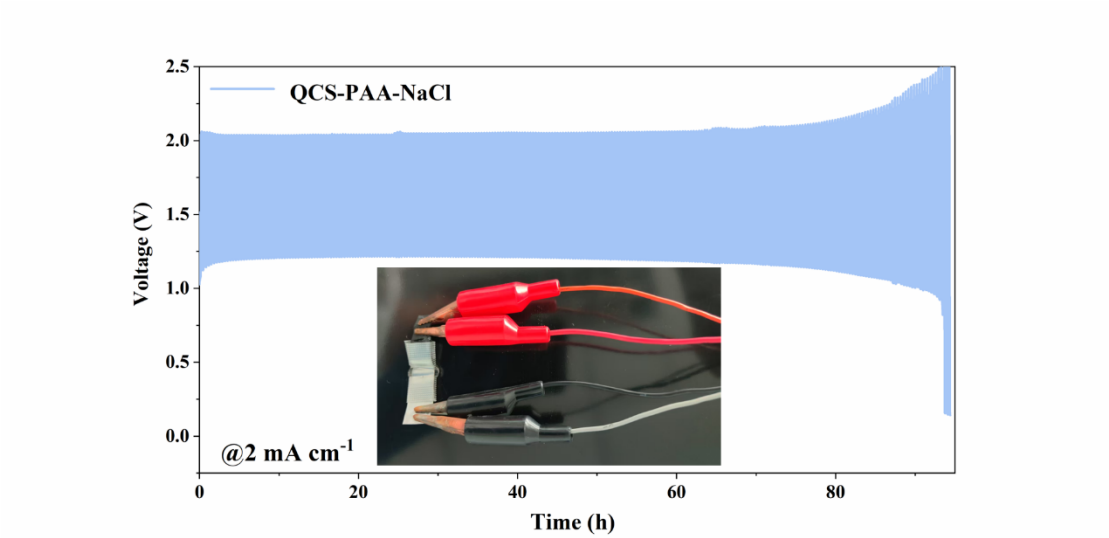

Figure S10. Cycling performance of the QCS-PAA-NaCl based ZAB under bending conditions.

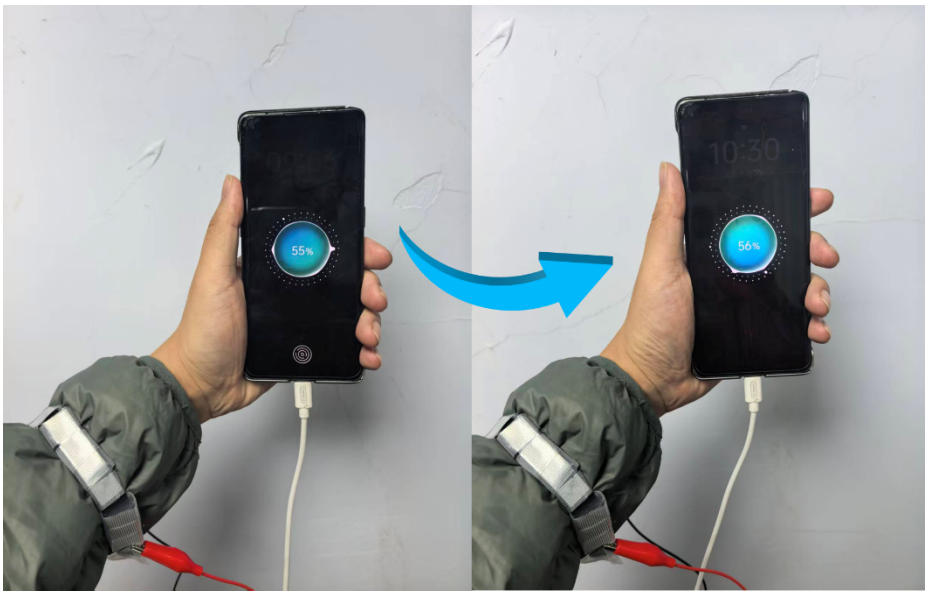

Figure S11. The assembled flexible ZABs powering a mobile phone under wearable conditions.

Table. S2 Performance Comparison of QCS-PAA-NaCl Based FlexibleZABs with Previously Reported Gel Based ZABs

Gel polymer electrolytes	**Conductivity (mS cm^{-1})**	**Power density (mW cm^{-2})**	**Cycle life (h)@2 mA cm^{-2}**	**Refs.**
QCS-PAA-NaCl	**217**	**68.5/-30°C** **114.2/20°C**	**470/-30°C** **115/20°C**	**This work**
PMA-HL0.02	130	113.2/RT	150/RT	Ref. 8
PAMA-ANa/Fe^{3+}	86	86/RT 65/-20°C	150/RT	Ref. 9
AA-AMPS-KCl	368	389.1/RT	55/RT	Ref. 10
PAG	86	60/RT 32/-40 °C	140/-40°C 48/RT	Ref. 11
PAM-PAZn-SE-CS	217	74.14/RT	168/RT	Ref.12
SPEEKG-Zn^{2+}	51	171.6/60°C	55/40°C 49/-20°C	Ref 13.
PAM-BBr	340	101.2/20°C	144/20°C 220/-30°C	Ref.14
P-SH/PAM	241	85.5/RT	28/RT	Ref.15
MF-LDHs@PVA	138	61.42/RT	35/Rt	Ref.16

References

1. Becke, A. D. Density-functional thermochemistry. III. The role of exact exchange. *J. Chem. Phys.,* 1993, **7**, 5648-5652.
2. Weigend, F.; Ahlrichs, R. Balanced basis sets of split valence, triple zeta valence and quadruple zeta valence quality for H to Rn: Design and assessment of accuracy. *Phys. Chem. Chem. Phys.,* 2005, **7**, 3297-3305.
3. Grimme, S.; Antony, J.; Ehrlich, S.; Krieg, H. A consistent and accurate ab initio parametrization of density functional dispersion correction (DFT-D) for the 94 elements H-Pu. *J. Chem. Phys.,* 2010, **132**, 154104.
4. Johnson, E. R.; Becke, A. D. A post-Hartree–Fock model of intermolecular interactions. *J. Chem. Phys.,* 2005, **123**, 024101.
5. Zhang, J.; Lu, T. Efficient evaluation of electrostatic potential with computerized optimized code. *J. Chem. Phys.,* 2021, **23**, 20323-20328.
6. Lu, T.; Chen, F. Multiwfn: A multifunctional wavefunction analyzer. *J. Comput. Chem.,* 2012, **33**, 580-592.
7. Lu, T. A comprehensive electron wavefunction analysis toolbox for chemists, Multiwfn. *J. Chem. Phys.,* 2024, **161**, 082503.
8. Liang, J.; Zhang, H.; Wan, L.; You, Z.; Li, C.; Wang, R.; Shang, Z.; Lei, D.; Li, Z. Gel polymer electrolytes based on compound cationic additives for environmentally adaptive flexible zinc-air batteries with a stable electrolyte/zinc anode interface. *Energy Storage Mate*r., 2024, **71**, 103677.
9. Shang, Z.; Zhang, H.; Liang, J.; You, Z.; Wang, R.; Wan, L.; Lei, D.; Li, Z. Highly

adhesive hydrogel electrolytes driven by adenosine monophosphate and Fe^{3+} for high-voltage asymmetric flexible zinc-air batteries. *Energy Storage Mater*., 2024, **71**, 103599.

10. Shang, N.; Wang, H.; Wang, K.; Zhang, R.; Zhong, D.; Wei, M.; Pei, P. A high power flexible Zn-air battery via concurrent PAA modulation and structural tuning. *Energy Storage Mater.,* 2025, **74**, 103923.
11. Zhang, S.; Tian, R.; Sun, Y.; Ji, Z.; Liu, Z.; Deng, H.; Liu, Y.; Hou, Y.; Jiang, Y.; Li, Q.; et al. Gelatin-based gel polymer electrolytes with high ionic conductivity for temperature adaptive flexible zinc-air batteries. *Int. J. Biol. Macromol*., 2025, **310**, 143218.
12. Zhao, Y.; Li, X.; Zhang, H.; Zhang, Z. Constructing dual-ionic channels to enhance the cycle stability of solid-state zinc-air batteries. *J. Energy Storage*., 2025, **115**, 115987.
13. Ren, Z.; Niu, J.; Zhang, X.; Liu, X.; Travas-Sejdic, J. Performance Regulation of Sulfonated Poly(ether ether ketone) for Preparing Multi-Adaptive Electrolyte and Battery Separator of Wide-Temperature Flexible Zn-Air Batteries. *Small Methods*.,2025, 2500884.
14. Zhang, J.; Song, X.-M.; Sun, Z.; Liu, D.; Song, Z.; Li, S. A multifunctional IL hydrogel electrolyte for zinc anode-stabilized flexible zinc-air batteries over a wide temperature range. *J. Energy Storage*., 2025, **125**, 116985.
15. Li, X.; Zhang, B.; Jiang, C.; Zhang, J.; Ning, X.; An, Z.; Chen, X.; Chen, Y.; Chen, P. Long cycle lifespan of flexible rechargeable zinc-air batteries based on

porous sodium hyaluronate/polyacrylamide-based hydrogel electrolyte. *J. Power Sources*., 2025, **641**, 236828.

16. Zeng, Y.; Gong, Y.; Wang, W.; Song, X.; Xiong, D.; Du, Y.; Zhou, L.; Cao, Y.; Zhan, F.; Liu, Y. A melamine foam-scaffolded LDHs@PVA gel electrolyte with high ionic conductivity and water retention capability for flexible zinc-air batteries. Green Chem., 2025, **27,** 14627.